Supporting Information

Constructing FeCoNi-LDH/MOF heterostructure as cocatalyst on hematite photoanode for highly efficiency water splitting

Qianyu Gao,[a,b] Yuhan Bai,[a,b] Peilin Song,[b] Qingwen Dong,[b] Jingjing Luo,[b] Shun Zhao,[b] Xiangwei Tian,[b] Xiu-Shuang Xing,[b*] and Jimin Du[a,b*]

[a]College of Chemistry, Zhengzhou University, Zhengzhou 450000, P. R. China. E-mail: djm@iccas.ac.cn

[b]International Joint Laboratory of Henan Photoelectric Functional Materials, College of Chemistry and Chemical Engineering, Anyang Normal University, Anyang 455000, P. R. China. E-mail: xsxing0621@163.com

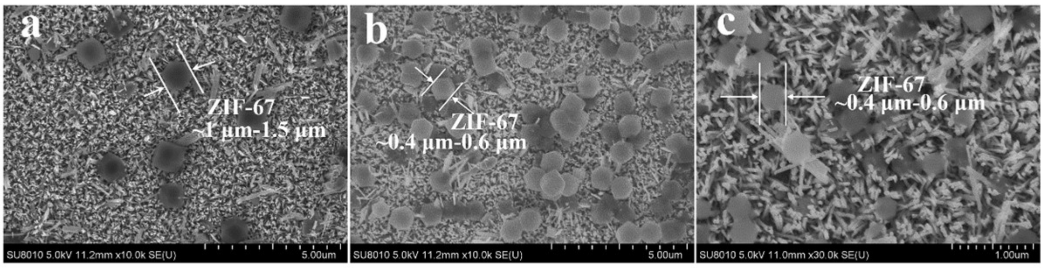

Figure S1. The view SEM images of Sn@α-Fe_2O_3/ZIF-67-R2 (a), Sn@α-Fe_2O_3/ZIF-67-R4 (b) and Sn@α-Fe_2O_3/ZIF-67-R8 (c) photoanodes.

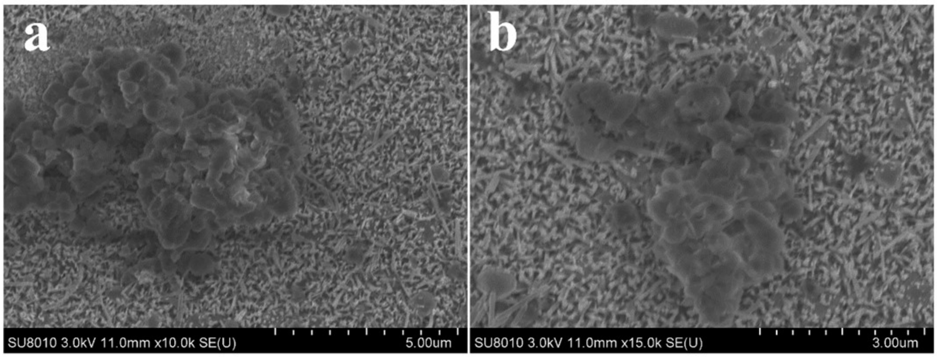

Figure S2. The view SEM images of Sn@α-Fe_2O_3/ZIF-67 photoanode during the hydrolytic collapse process under urea condition.

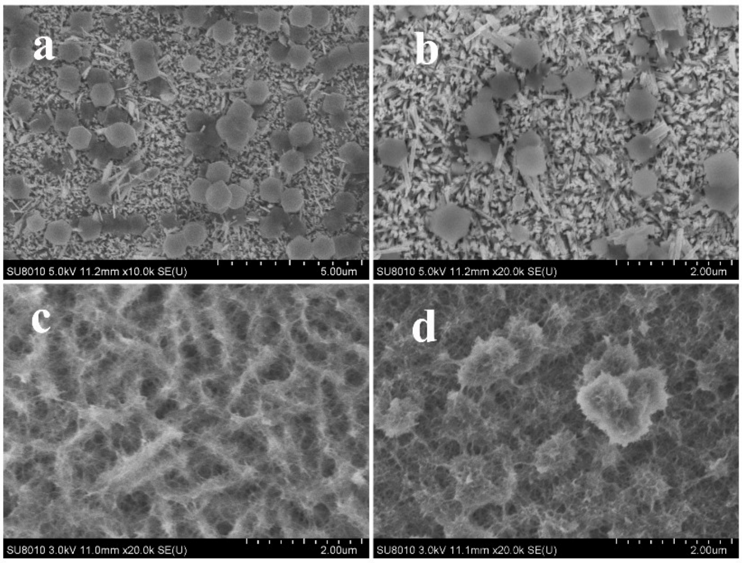

Figure S3. The SEM images in the top view of Sn@α-Fe_2O_3/ZIF-67 at 10K (a), Sn@α-Fe_2O_3/ZIF-67 at 20K (b), Sn@α-Fe_2O_3/FeNi-LDH (c), and Sn@α-Fe_2O_3/ZIF-67/FeCoNi-LDH (d) photoanodes.

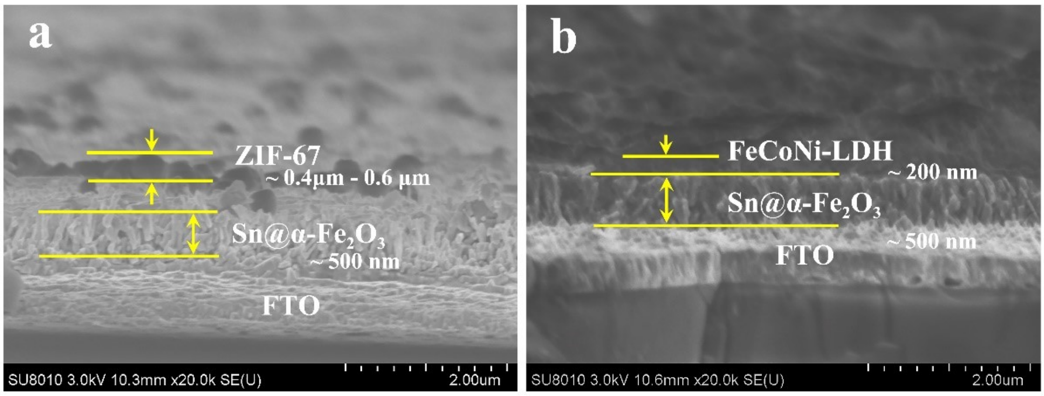

Figure S4 The cross-sectional SEM images of (a) Sn@α-Fe_2O_3 and (b) Sn@α-Fe_2O_3/ZIF-67/FeCoNi-LDH photoanodes.

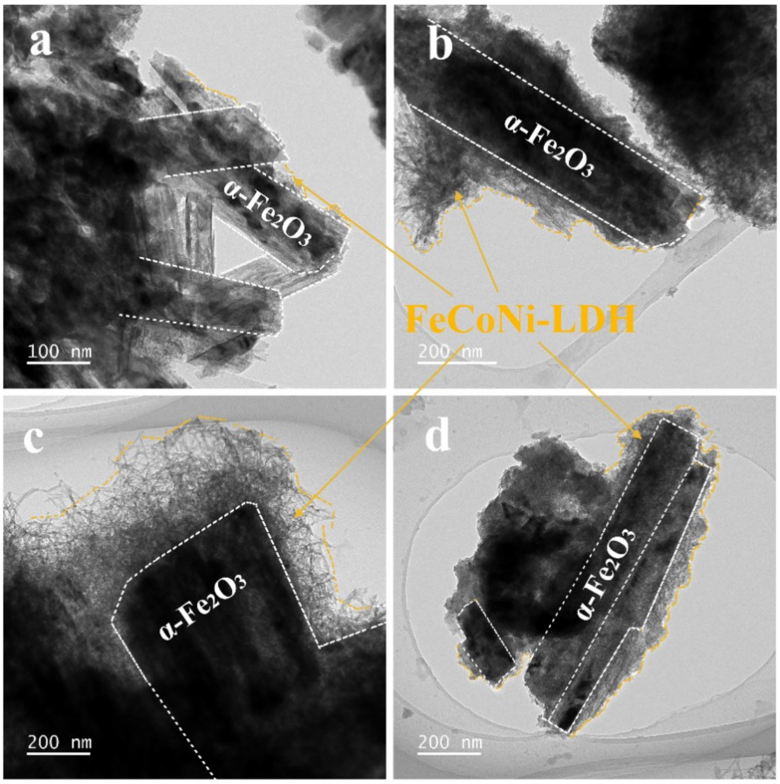

Figure S5. TEM images of Sn@α-Fe_2O_3/ZIF-67/FeCoNi-LDH photoanode.

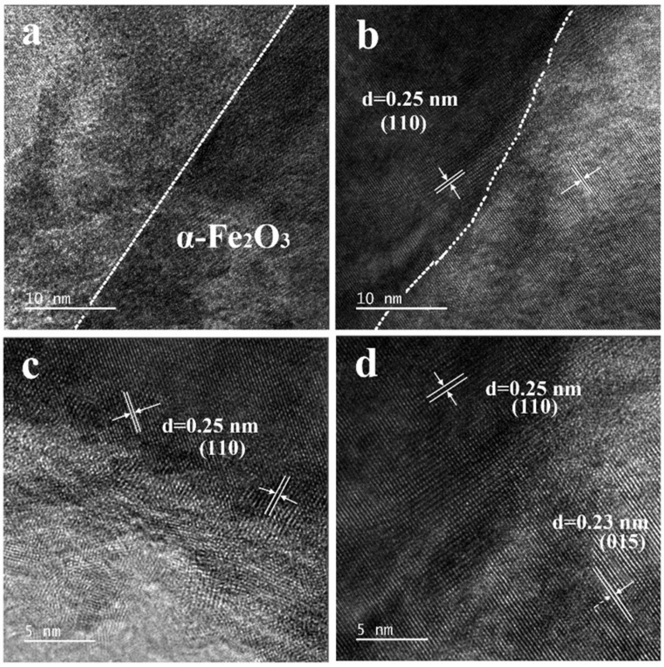

Figure S6. HRTEM images of Sn@α-Fe_2O_3/ZIF-67/FeCoNi-LDH photoanode.

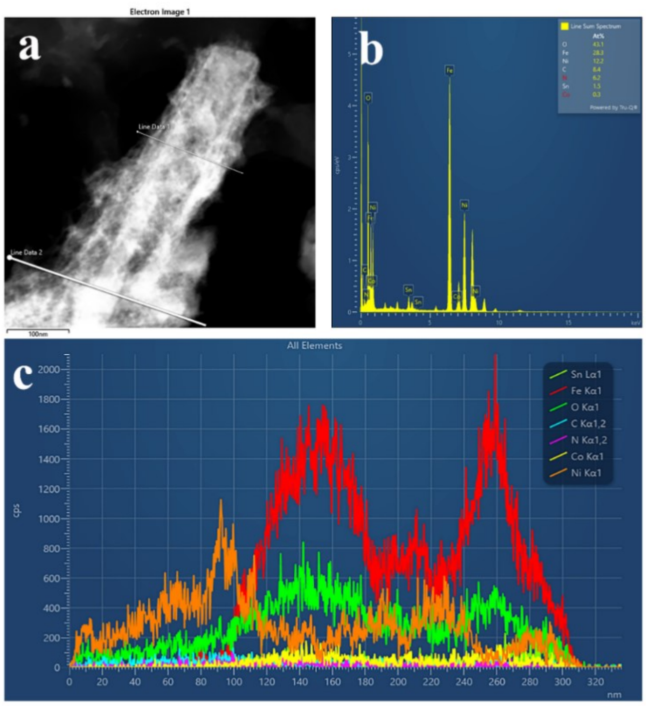

Figure S7. (a) Electron image; (b) The element composition in line sweep; (c) Elements linear scanning image of Sn@α-Fe_2O_3/ZIF-67/FeCoNi-LDH photoanode.

Table S1. Element composition of Sn@α-Fe_2O_3/ZIF-67/FeCoNi-LDH photoanode.

Element	Line Type	k Factor	Wt%	Wt% Sigma	Atomic %
C	K series	3.115	8.22	0.31	21.20
N	K series	1.807	2.05	1.06	4.52
O	K series	1.455	19.13	0.35	37.02
Fe	K series	1.214	38.84	0.52	21.53
Co	K series	1.286	0.54	0.12	0.28
Ni	K series	1.293	27.37	0.41	14.44
Sn	L series	1.890	3.85	0.22	1.00
Total:			100.00		100.00

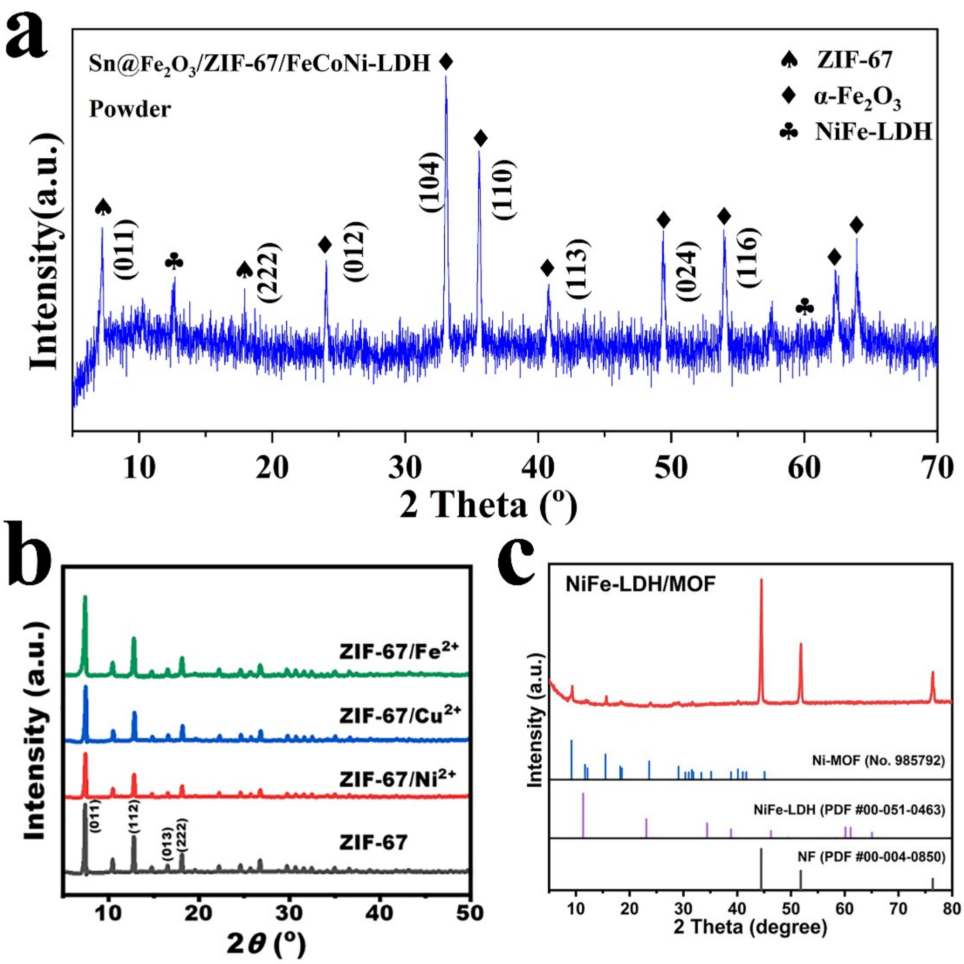

Figure S8 (a) XRD pattern of a powder sample of Sn@α-Fe_2O_3/ZIF-67/FeCoNi-LDH photoanode; (b) The XRD patterns of ZIF-67 in the reported reference [*Chem. Eng. J.*, 2023, 465, 142703]; (c) The XRD patterns of NiFe-LDH in the reported reference [*Nano Res.*, 2023, 16, 8945-8952].

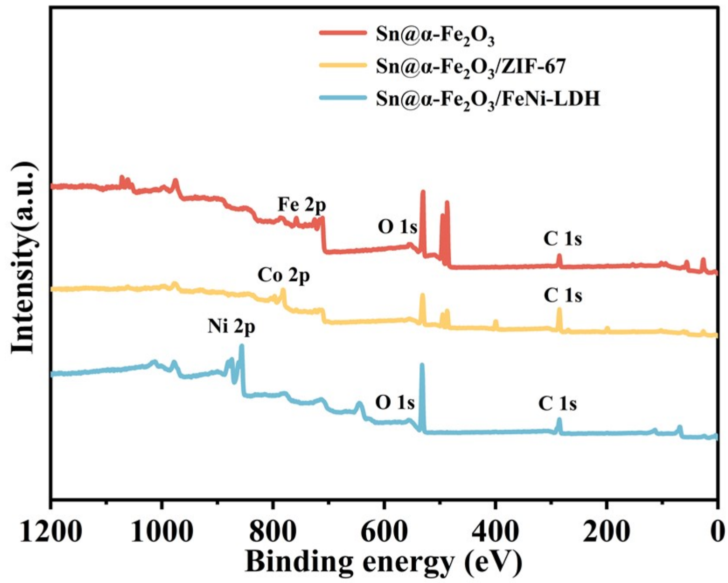

Figure S9. The XPS patterns of Sn@α-Fe_2O_3, Sn@α-Fe_2O_3/ZIF-67, and Sn@α-Fe_2O_3/FeNi-LDH photoanodes.

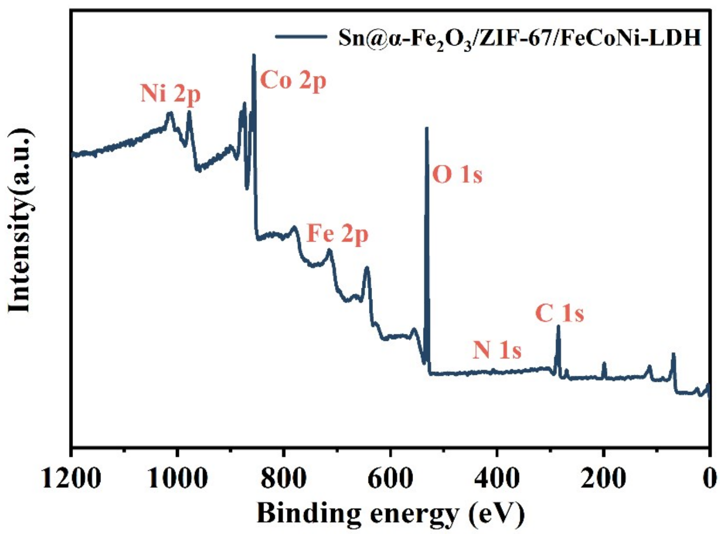

Figure S10. The XPS pattern of Sn@α-Fe_2O_3/ZIF-67/FeCoNi-LDH photoanode.

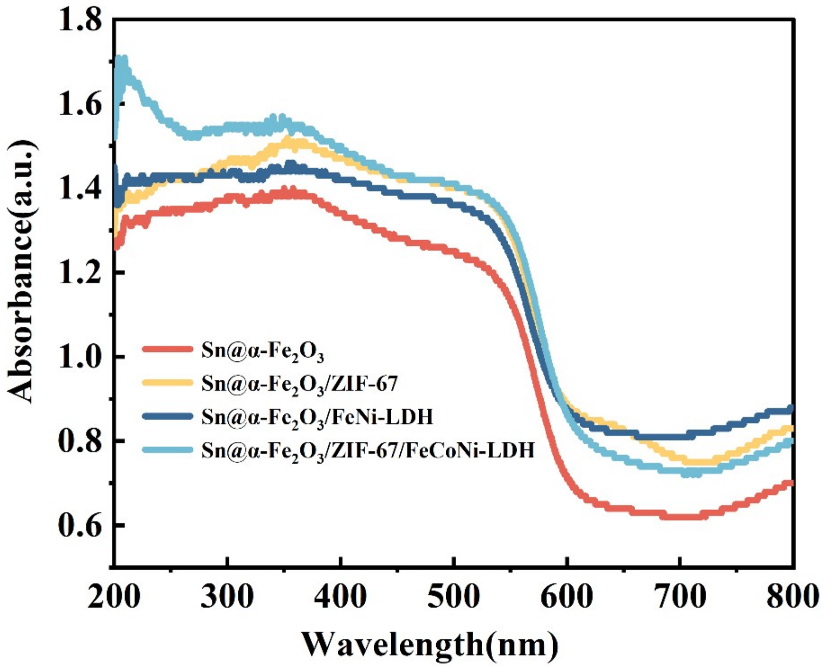

Figure S11. The UV-vis absorbance spectra of Sn@α-Fe_2O_3, Sn@α-Fe_2O_3/ZIF-67, Sn@α-Fe_2O_3/FeNi-LDH and Sn@α-Fe_2O_3/ZIF-67/FeCoNi-LDH photoanodes.

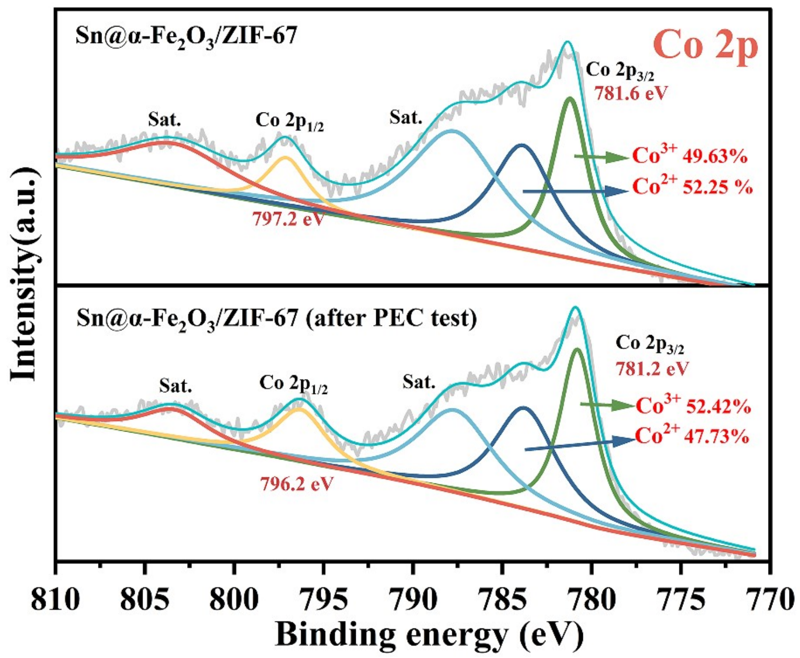

Figure S12 XPS spectra of Co 2p of Sn@α-Fe_2O_3/ZIF-67 photoanode before and after the PEC reaction.

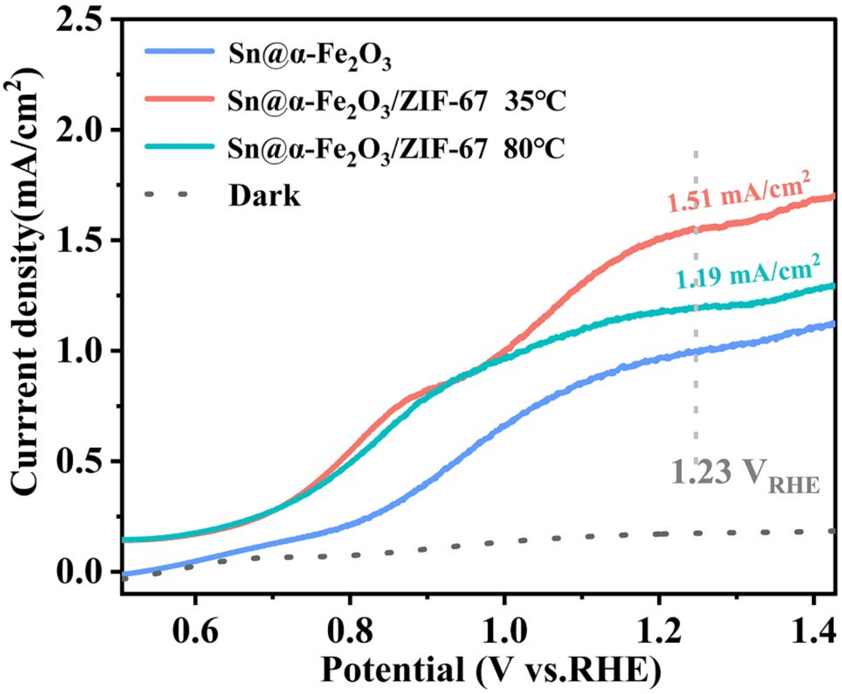

Figure S13 The *J*-*V* curves of Sn@α-Fe_2O_3/ZIF-67 photoanodes at different temperature.

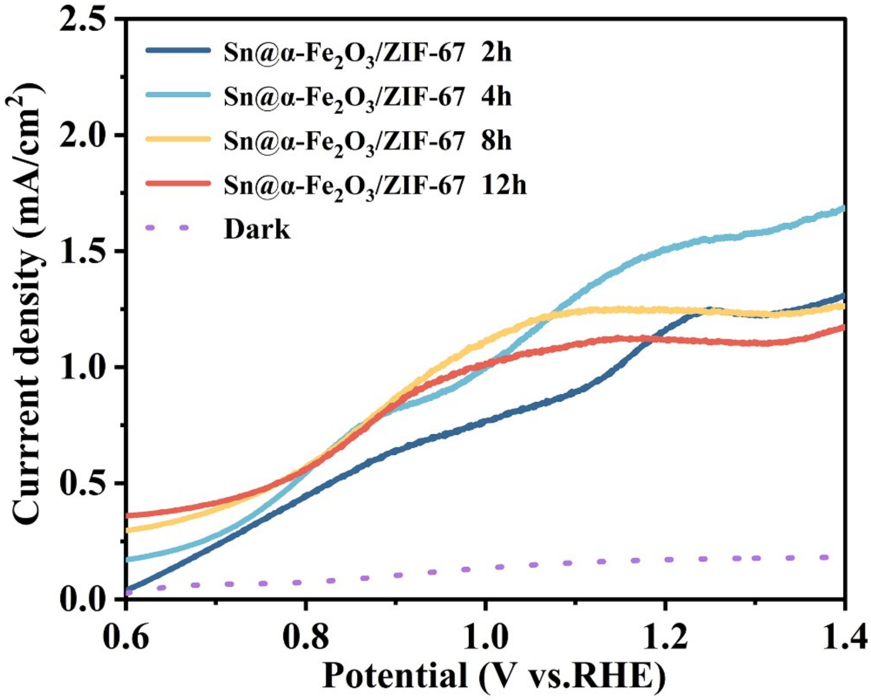

Figure S14 The *J*-*V* curves of Sn@α-Fe_2O_3/ZIF-67 photoanodes at different reaction times.

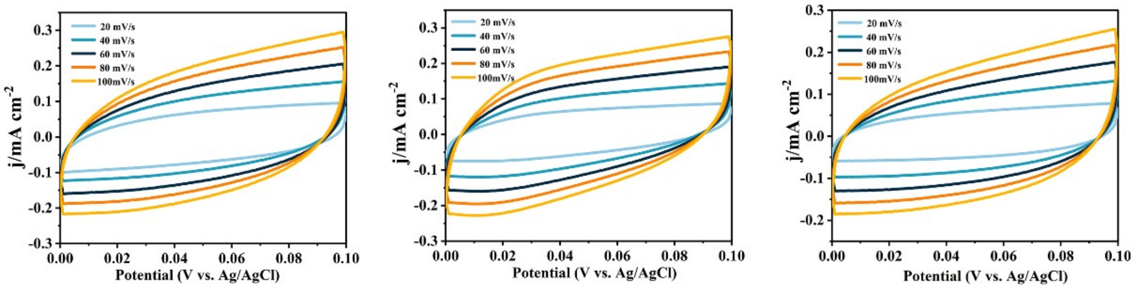

Figure S15. CV curves for Sn@α-Fe_2O_3, Sn@α-Fe_2O_3/ZIF-67 and Sn@α-Fe_2O_3/FeNi-LDH photoanodes.

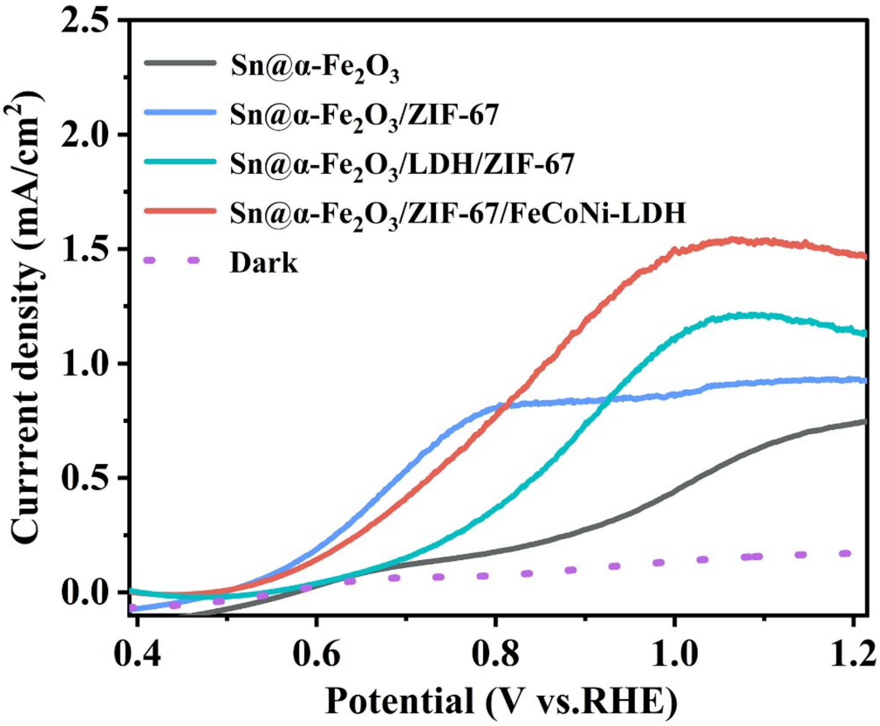

Figure S16 *J-V* curves of Sn@α-Fe_2O_3, Sn@α-Fe_2O_3/ZIF-67, Sn@α-Fe_2O_3/LDH/ZIF-67 and Sn@α-Fe_2O_3/ZIF-67/FeCoNi-LDH photoanodes.

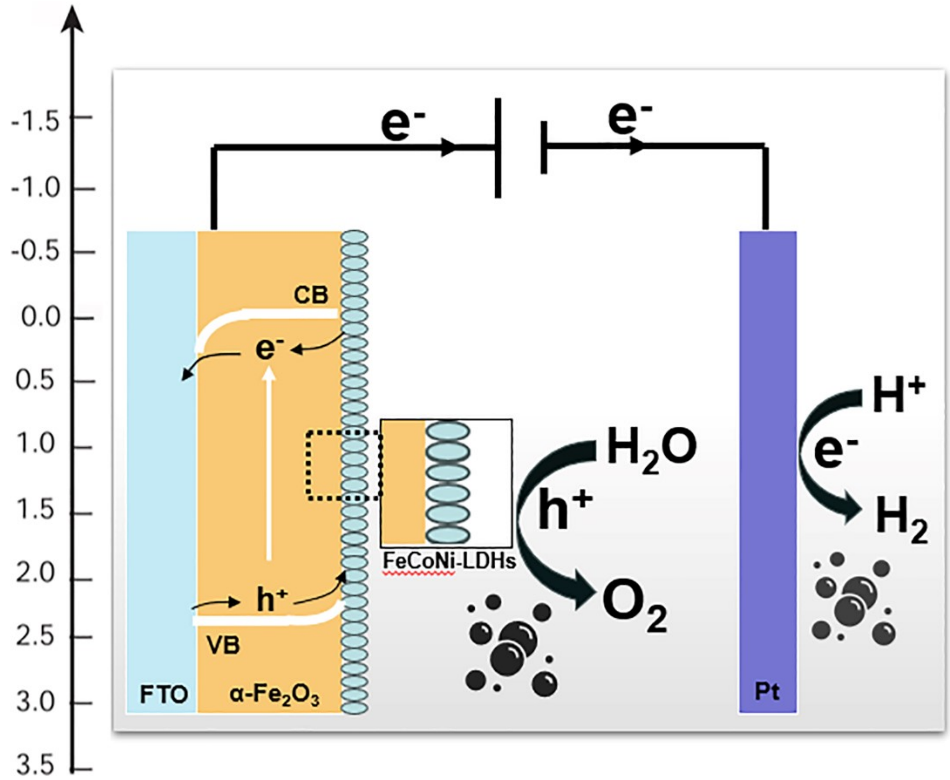

Figure S17 Schematic diagram of the reaction mechanism of PEC water oxidation for α-Fe_2O_3 photoanode modified with FeCoNi-LDH cocatalyst.